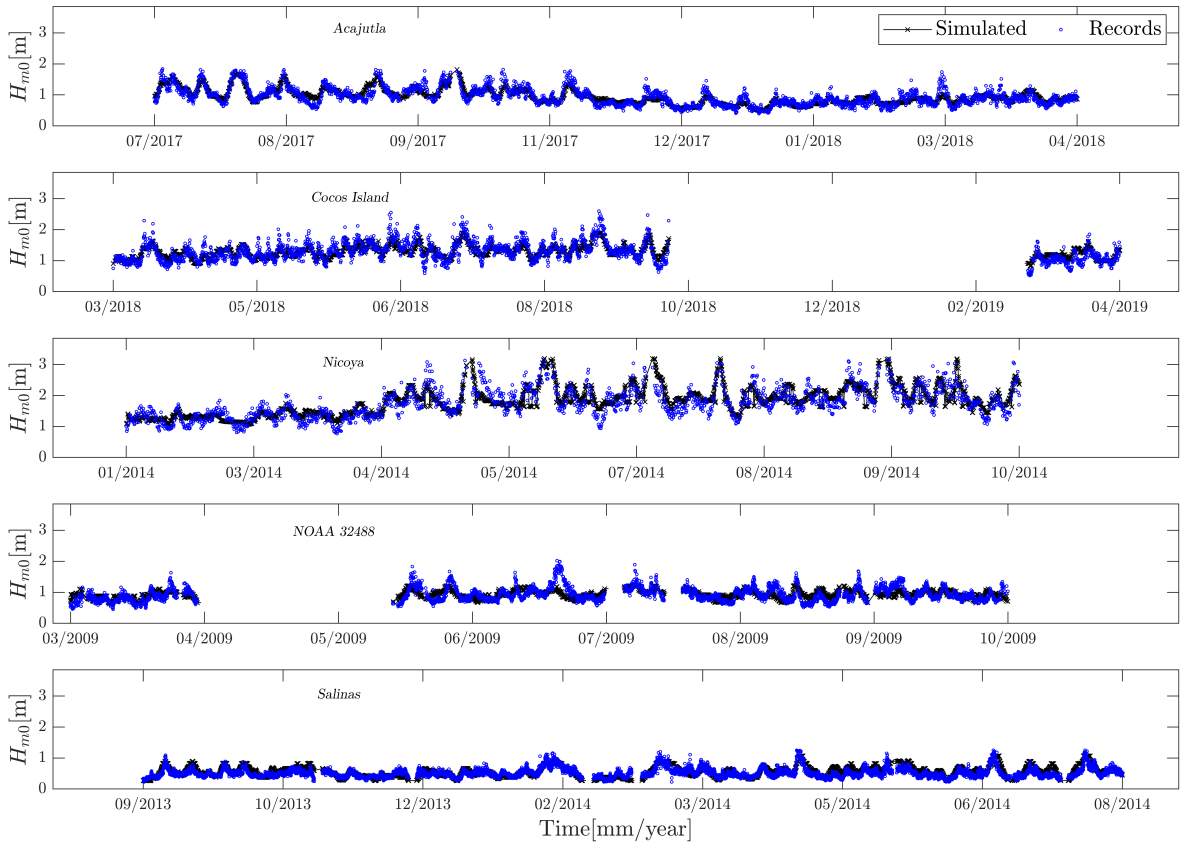

Figure 2.9: Time series of the H_{m0} modelled data against the in-situ data at 5 nearshore locations.

events. In this case, the worst adjustment as found at the Cocos island buoy where the $RMSE$ value is 22.20°, while the best $RMSE$ was found in Acajutla with a value of 7.90°. $RMSE$ values in between of 13.2° and 18.9° were found in the rest of the locations.

In general, there was not found a relevant improvement, as that one obtained for the H_{m0}, in the correction quality respect to the latitudes neither in time window given the poor temporal coincidence between in-situ records, where perhaps certain meteoceanic events reflect any specific trend. Even if uncertainties exist the database can be employed given that the bias have shown to be low, e.g. in the H_{m0} were lower than 0.01 m, in the case of T_P the highest bias corresponds to 2.17 s, and the highest bias for D_P corresponds to 13.60 °.

After testing and evaluating the numerical model in the region, we proceeded with the applicability of the generated wave information, such as the wave energy assessment. It was found that in periods where H_{m0} records were high there exists a less accurate adjustments of the modelled and corrected data, suggesting that a extreme events may be analyze separately. However, the mean regime of H_{m0}, T_p, and D_p fit acceptably based on the results presented in this section.

The wave modelling can be extended for the production a wave forecasting database, by ensuring a proper quality of the input data, i.e. the accuracy would be directly linked to the wind input and bathymetry datasets. Likewise, as observed in this study a further analysis regarding the wave storms periods must be performed in order to offer more validity to the

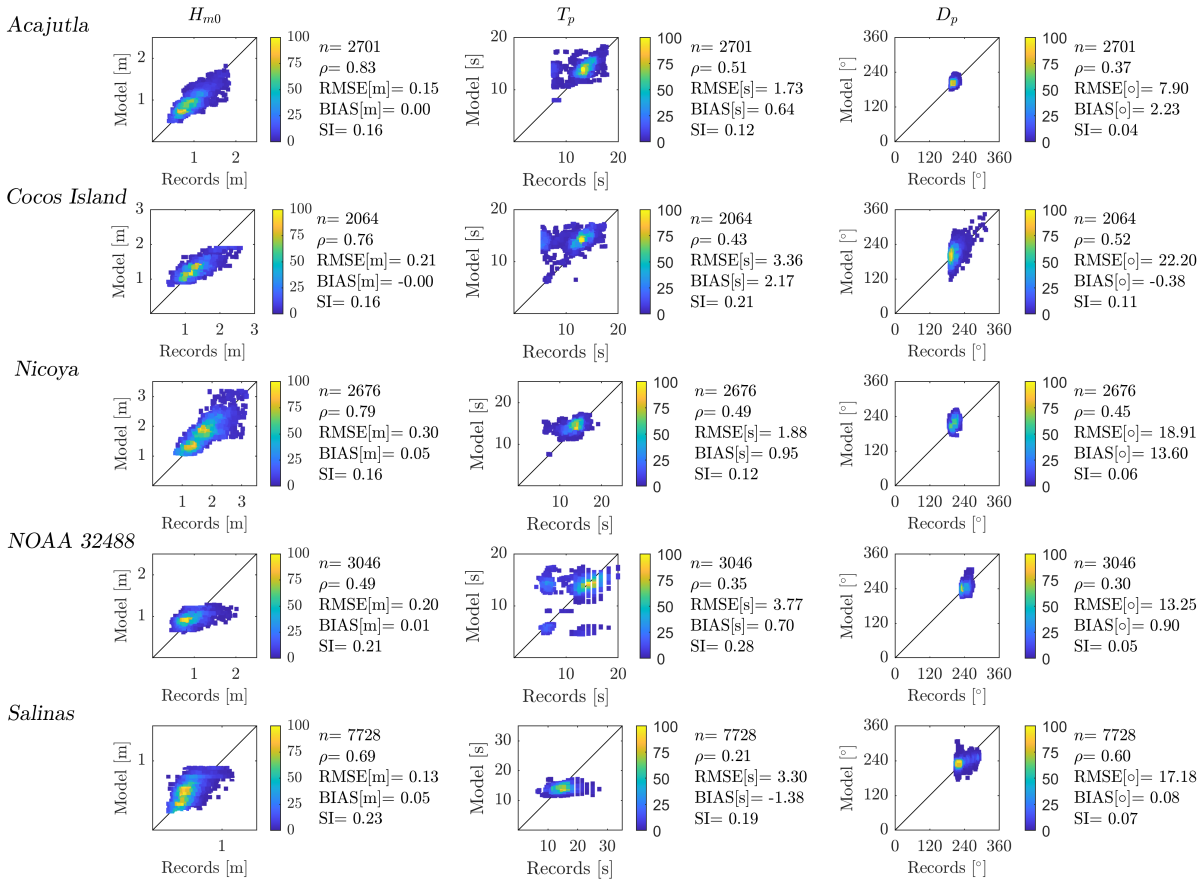

Figure 2.10: Scatter plots of the modelled data against the in-situ data.

Table 2.7: Adjustment statistics of the validation data: H_{m0}, T_p and D_p.

Locations	n	H_{m0}			T_p			D_p		
		ρ	$RMSE$ [m]	SI	ρ	$RMSE$ [s]	SI	ρ	$RMSE$ [°]	SI
Acajutla	2701	0.83	0.15	0.16	0.51	1.73	0.12	0.37	7.90	0.04
Cocos Island	2064	0.76	0.21	0.16	0.43	3.36	0.21	0.57	22.31	0.11
Nicoya Peninsula	2676	0.79	0.49	1.88	0.49	1.88	0.12	0.45	18.91	0.06
NOAA 32488	3046	0.49	0.20	0.21	0.35	3.77	0.28	0.30	13.25	0.05
Salinas	7728	0.69	0.13	0.23	0.21	3.30	0.19	0.60	17.18	0.07

predicted wave data.

Further applications of the wave hindcasting developed in this study include complementary studies of temporal and spatial trends of the main parameters, under the optimised configuration, directional energy density spectra could be recalculated for analysis.

2.4. Final remarks

An optimized wave hindcasting database was generated, with hourly outputs from January 1980 to August 2021, under an unstructured mesh increasing its spatial resolution until the Central American shoreline is reached, wherein the nodes separation is 1 km. The wave hindcast produced provides hourly integral parameters over the computational domain. These parameters are: bulk-based corrected H_{m0}, T_p, spectral mean periods (Tm_{01} and Tm_{02}), wavelength (λ_w), wave directional spreading (σ_D), direction of wave propagation associated to the peak period (D_p), wind sea fraction (tws), wind speeds at 10 m height (x-component U_w and y-component V_w).

After evaluated several run test by varying the WWIII parametrizations it was found that the ST4 and ST6 produces near results of H_{m0} among the run tests, where the ST4 offers a better adjustment to the satellite records for the bulk correction procedure of H_{m0}.

It is concluded that the employed 2-step H_{m0} correction process (bias adjustment of the cumulative H_{m0} distribution followed by the adjustment method published by Albuquerque et al. [2018]), has produced satisfactory adjustments based on the results reported in Table 2.5. In nearshore regions the partitioned-based correction has shown to estimate more accurate the H_{m0} than the bulk correction.

Besides, the evaluation of both wind input datasets into the WWIII model has indicated slight differences on the results of H_{m0}, as demonstrated by the comparison between run10 and run12 statistics of Table 2.5. A relative error of the mean ρ of all nodes between the run10 and run12 is about 1.5 %.

The comparison of different fitting parameters for the assessment of seabed friction, as well as the consideration of the turbulent regime at the water surface, i.e. GAMMA, and SWELLF6 and SWELLF7 in Table 2.3 respectively, did not improve significantly the results. The aforementioned is concluded after having observed the Taylor diagrams in Figure 2.7.

Furthermore, it was observed that the fit statistics for each parametrization vary depending on whether the location of the nodes is considered deep or shallow water. The second row of charts in Figure 2.7 presents how the different model parametrizations statistics vary, most of them not significantly. Particularly, the test run 10, considered the optimal parametrization, it produces ρ values which differs less than 3.5% through the classification of all, deep water or shallow water nodes. The Pearson correlation coefficient passed from 0.7971 at the averaged deep waters nodes (Figure 2.7 (E)) to all the averaged nodes considered to a value of 0.7729 (Figure 2.7 (D)) which is still representative for the shallow waters nodes (Figure 2.7 (F)). Such variations in the statistics for each node are presented through the Figure 2.8.

Moreover, although in shallow water the highest Pearson correlation coefficient corresponds to run 9 (ρ=0.7569), run 10 (ρ=0.7556), as indicated in Table 2.5, is employed as the optimal parametrization for estimating the entire wave hindcast since it does not differ significantly from run 9.

Finally, several applications can be developed based on the results obtained in this wave hindcasting data such as wave climate analysis, assessment on wave extreme events, further wave propagation and downscaling over localised coastal domains, as well as the generation of a wave forecasting database over the Pacific of Central America.